Cable-Controlled Aeroshell Deceleration System

University of Illinois at Urbana-Champaign

Department of Aerospace Engineering

104 S. Wright Street

Urbana, Illinois 61801

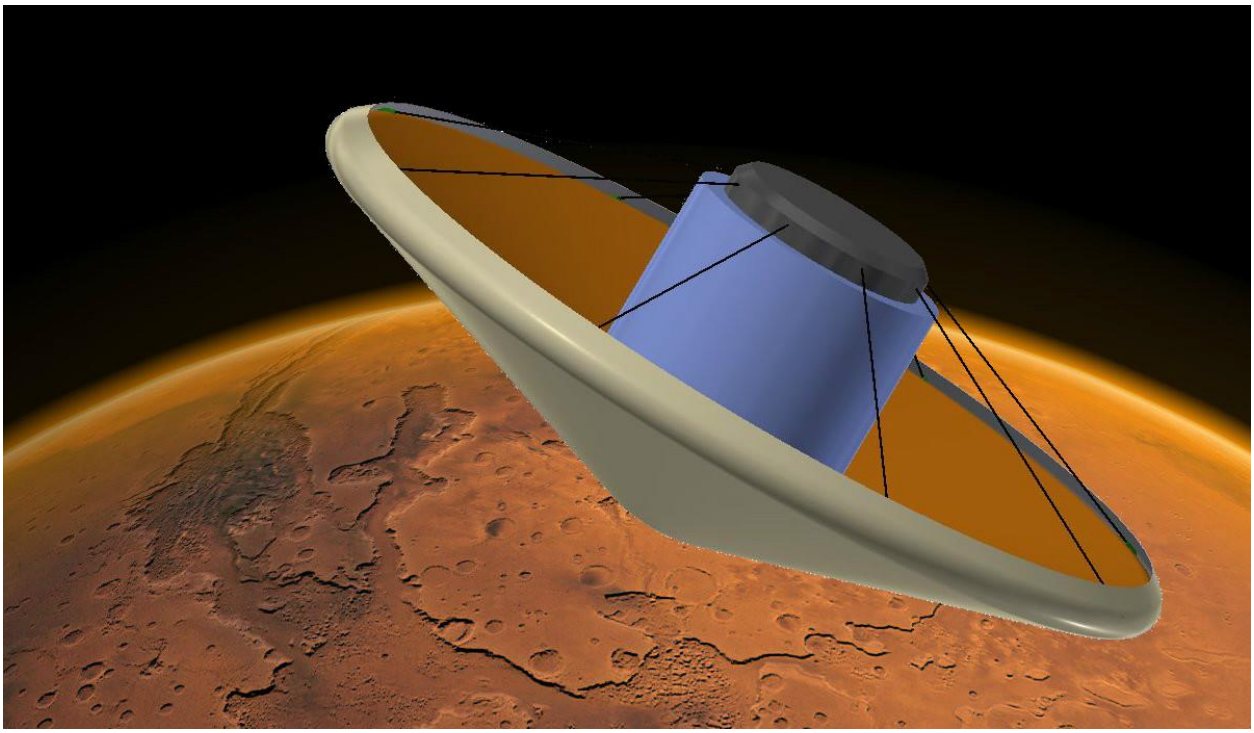

Team Members:

Sashank Gummella, *Aerospace Engineering, Sophomore*

Steven Kosvick, *Aerospace Engineering, Sophomore*

Austin Scott, *Aerospace Engineering, Sophomore*

Jose Tuason, *Aerospace Engineering, Senior*

Sam Wywrot, *Aerospace Engineering, Sophomore*

Faculty Advisor:

Zachary Putnam, *Aerospace Engineering*

1. Introduction

By utilizing a system of cables capable of withstanding extreme conditions, the BIG Idea team at the University of Illinois at Urbana-Champaign has designed a HIAD control system capable of precise control of both human and robotic vehicles entering the Mars atmosphere. The Cable-Controlled Aeroshell Deceleration System (CCADS) is designed to morph the aeroshell of the HIAD in such a way as to guide the entry vehicle during its descent towards the Mars surface.

2. CCADS Concept

The HIAD aeroshell will pressurize above the Mars atmosphere in an initially flat configuration. Prior to entry, the CCADS will utilize tension in the cables to morph the entire aeroshell such that the half-cone angle between the aeroshell and the payload compartment is 65 degrees. The equilibrium configuration of the aeroshell will be maintained as the entry vehicle descends from approximately 125 km to 50 km above the Mars surface, at which altitude the density of the atmosphere will be thick enough to allow for effective control over the lift-to-drag ratio of the HIAD. Any tension applied to the cables will be produced by the electric motor in the top section of the payload compartment.

2.1 Mission Profile (50 km to 11 km altitude)

When the entry vehicle approaches an altitude of approximately 50 km, where the density of the Mars atmosphere begins to increase substantially, morphing the cross-section of the aeroshell can have an effect on the flight path angle and trajectory of the entry vehicle. Based upon the target landing area, the aeroshell can be morphed in such a way that flight path alterations and trajectory changes can guide the entry vehicle to that location.

Once the entry vehicle is decelerated to supersonic speeds below Mach 2.0, at an altitude of approximately 11 km, terminal descent will be initiated to slow the vehicle further and perform a safe landing. An isothermal Mars atmosphere was assumed between 11 km and 50 km with a temperature of 210 K. Given this temperature, the torus can be pressurized between 3 and 5 psi. Since the pressure applied by the drag force is far less than the minimum pressure required for morphing the torus, the effect of drag in counteracting the natural tendency of the aeroshell to return to a natural state of equilibrium during cable slackening is negligible. In other words, the drag force could not apply enough pressure to prevent the aeroshell from returning to its natural state of equilibrium. By slackening the tension in the cables, the aeroshell will return to a configuration with a half-cone angle of approximately 65 degrees.

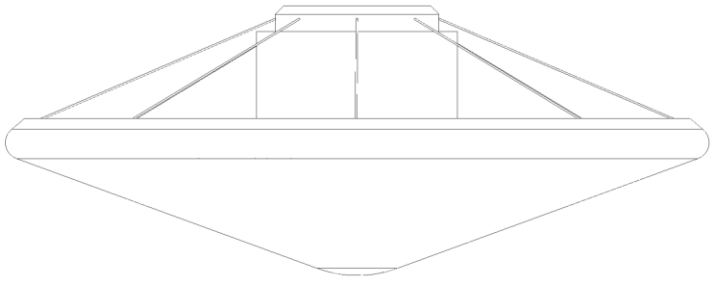

Figure 1. Axial view of the entry vehicle.

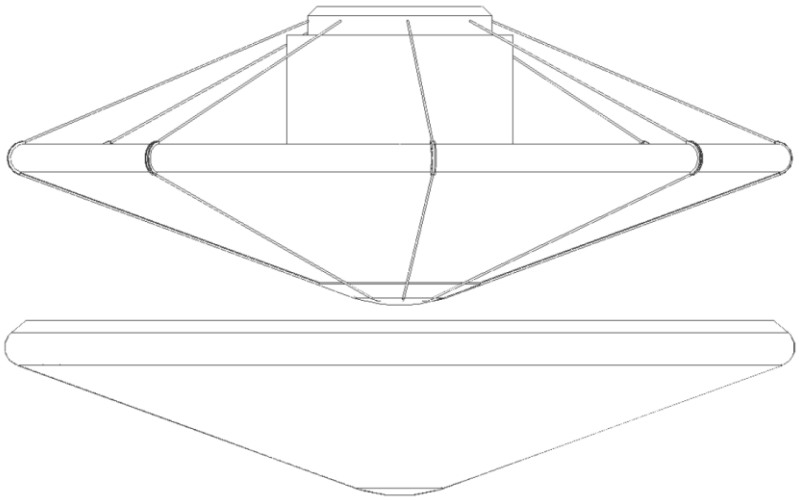

Figure 2. Axial views of the cable configuration of the CCADS (top) and the single inflatable torus (bottom).

2.2 Cables

2.2.1 Material

After having further analyzed the design of the CCADS, one issue that was identified was the cable material. Though titanium was originally considered as a hypothetical candidate for the cable material given its high ultimate strength, and low thermal expansion, scientific evaluation of material properties demonstrates that Kevlar 29 or Kevlar 49 cables will be ideally suited to facilitating mission concept of the CCADS.

Kevlar's tensile strength, coefficient of thermal expansion, and endurance directly enhance the mission objectives and design concept of the CCADS. While Kevlar 29 and Kevlar 49, variants for Kevlar yarn, begin to experience weight loss and deterioration between 427 degrees and 482 degrees Celsius, amending this issue would enable Kevlar's use in the CCADS. More specifically, the part of the cables exposed to the atmosphere during entry would need to be coated with heat resistant shielding to protect the cable, itself. Adding the heat resistant coating would only ensure that Kevlar will survive entry temperatures of approximately 400 degrees Celsius. Given a density of .052 lb/in^3 and a tenacity range of 424 psi to 435 psi, the specific tensile strength of Kevlar is between $8.15x10^6$ in and $8.37x10^6$ in, about eight times greater than that of steel cables. The Kevlar cables will most likely be able to support the load of the aeroshell given the enumerated tensile strengths.

Though other high-tensile strength materials like S-Glass and Nylon-66 have been used in wire ropes, Kevlar provides the best balance of the mechanical properties surveyed. Ultimately, Kevlar will retain its properties of high yield strength and low elastic modulus at the temperatures that are expected to affect the entry vehicle. Between 149 and 177 degrees Celsius, Kevlar yarn retained a tensile strength of more than 250,000 psi over a time period of approximately forty hours. Given a circular cross-sectional area of 4π in^2, each cable would, theoretically, be able to support more than 3 million pounds of force between 149 and 177 degrees Celsius for an extended period of time before breaking. Given this statistic, it can be surmised that each cable would be more than capable of supporting part of the aeroshell's circularly distributed weight and tendency to retain naturally flatter configuration.

Since the cables will have to remain coiled in the entry vehicle for the duration of the entire Earth-Mars transfer phase, plastically deforming the cables prior to use would ensure that no sudden

deformation would occur during deployment of the CCADS, and would optimize the cable tension. Braided Kevlar was even used as a tether between the drag chute and lander during the descent phase of the Mars Pathfinder mission.

2.2.2 Electric Motor

The team members were also able to determine that the second electric motor, originally situated in the lower section of the payload compartment, was obsolete in the role that it was supposed to fulfill, which was to apply tension to the cables such that the applied tension from the top electric motor could, using control algorithms, be counteracted, balanced, and controlled more effectively. It was found that the second electric motor would not need to morph the aeroshell structure in such a way as to increase the half-cone angle between any single part of the aeroshell and the payload compartment. In other words, if, for example, tension was being applied by the cables to the torus to maintain a minimized cross section, then slackening the cables and decreasing the tension, alone, would result in the aeroshell effectively counteracting the slackening tension in the cables.

The electric motor in the top section of the payload compartment is part of the CCADS, and will apply tension to the cables to morph the aeroshell. Brushless DC (BLDC) motors, in contrast to AC, brushed DC (BDC), and stepper motors, are more efficient operating in the vacuum of space and under entry conditions. More specifically, BLDC motors are capable of operating at very high velocities and producing at least twice as much output torque as a BDC motor of the same size. In terms of mechanical simplicity, several small BLDC motors will be implemented to operate as many cables, individually. Ideally, each motor would, therefore, operate and fail independently of the other motors.

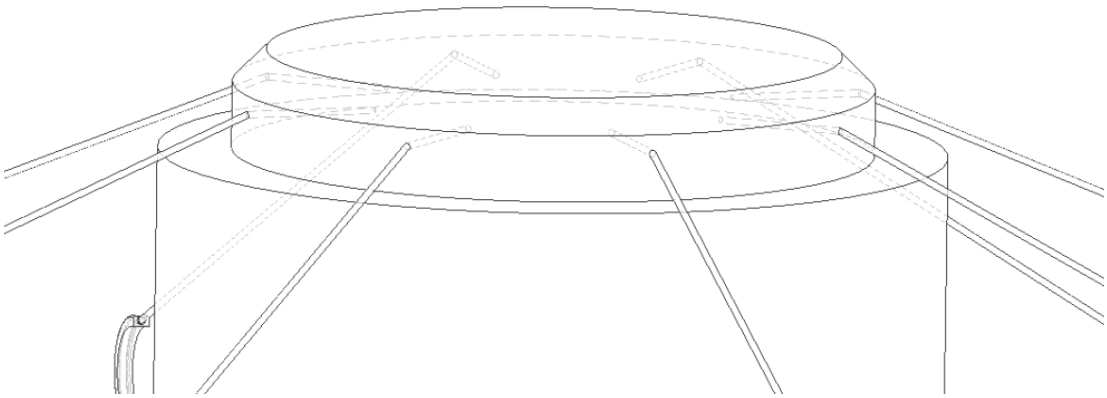

Figure 3. Cables are pulled by the motor through openings at the top of the payload.

2.3 Aeroshell

In addition, it was deemed more advantageous for control purposes to use a single inflatable torus as opposed to multiple tori in the aeroshell, itself. The reason for this design change is based on the fact that morphing a single torus would facilitate shape-morphing, and would also eliminate the risk of possibly dismantling the aeroshell. This inflatable torus would be inflated to a nominal 3 to 5 psi, despite the fact that it was estimated that 20 psi would optimize the performance of the aeroshell in entry conditions. This nominal range is based off the specifications of the existing IRVE-3. In fact, pressurizing

the torus to within the nominal range would also reduce the chances of structural pinching, whereby morphing the aeroshell could cause it significant damage.

2.4 CG-Offset Mechanism

To accommodate the much larger payloads that could be transported on a entry vehicle utilizing HIAD technology, the power supply necessary for operating the CG-offset mechanism (COM) would have to be much greater than that on the IRVE-3 craft. The proposed design would require a DC motor that would be more power-intensive and, consequently, more massive to offset the much larger payloads that the entry vehicle would transport through the atmosphere. Shifting mass would change the trim angle of the vehicle, thereby making it easier to change the magnitude of the lift vector of the entry vehicle during its descent.

2.5 Gutters

To ensure that the cables will remain laterally stationary as the electric motor applies tension, gutters will be attached to the aeroshell structure to not only guide the motion of the cables, but also to prevent the cables from sliding against the restraint wrap and causing wrinkling. These gutters will traverse the radius of the aeroshell, whereby the gutters will run radially outward from the nose of the forebody to the outer section of the torus, where the cables are exposed to the atmosphere. The gutters will be attached to the sides of inflatable torus and will be protected by the FTPS, which will cover the gutter. To minimize wrinkling in the FTPS as it stretches over the morphing aeroshell, the gutters are designed to be as flush with the aeroshell surface as possible, to avoid protruding into the FTPS and causing wrinkling.

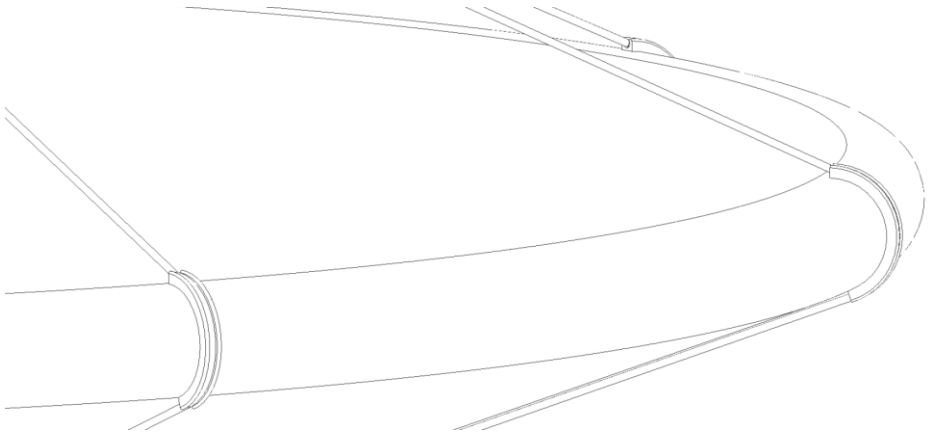

Figure 4. The cable gutters begin at the curvature of the inflatable torus.

2.6 Methods of Cable Attachment

In the white paper, it was not specified whether or not the cables that stretched from ports in the top section of the payload compartment to the aeroshell structure would be protected from overheating by the FTPS. Though our diagrams showed that the sections of the cables that lay against the forebody were not exposed to the atmosphere and were concealed by the FTPS, itself, this major design aspect was not explicated in the paper. At one end, the cables are attached to the pulley mechanism of the electric motor in the top section of the payload compartment. At the other end, the cables are attached to an anchor point of sorts, located in the lower section of the payload compartment. The cables are passed through small

ports in the hard cap at the bottom of the payload compartment, and are attached to hard attachment/anchor point situated in the lower section of the payload compartment. The FTPS will protect this hard cap as well as the cables passing through the ports. This configuration guarantees that tension in the cables can be applied to move and orient the aeroshell in various ways.

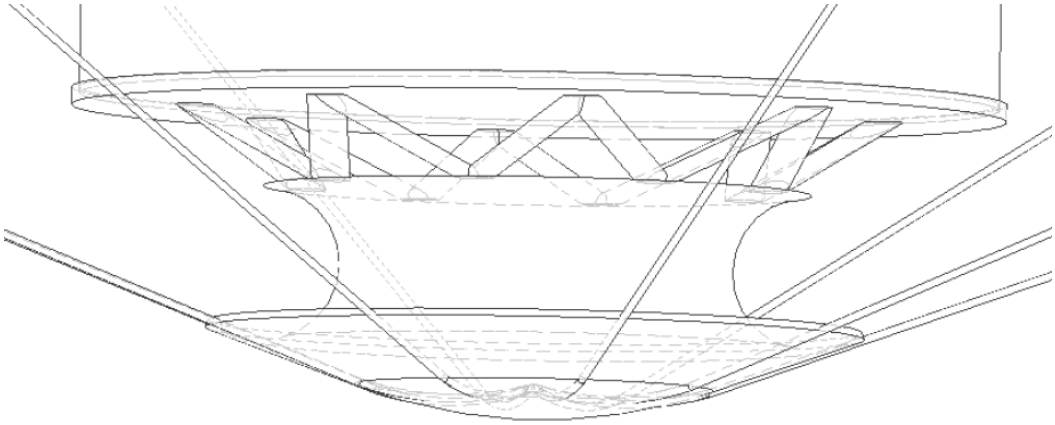

Figure 5. The cables pass through ports in the hard cap and upwards towards the anchor point.

2.7 Scalability of HIAD System

The cross-sectional area of the HIAD may be scaled up by a factor of as much as 44 from the original area of the IRVE-3. This was calculated by dividing the cross-sectional area of the HIAD (100π m^2) for this mission concept, by that of the IRVE-3 (2.25π m^2). The payload compartment can be scaled based upon the dimensions of the payload that is being transported by the entry vehicle. Components such as the FTPS must be scaled, but the degree to which the thickness of the FTPS is altered from that of the IRVE-3 depends on the present cross-sectional area of the HIAD. Incorporating the CCADS would require a new thickness of approximately 0.5 mm. It was found that 0.4 mm of pyrogel, in addition to thin layers of nicalon, kevlar, and kapton, would amount to a total FTPS thickness of approximately 0.5 mm. The required thickness of the pyrogel layer of shielding is calculated in section 3.4.

Since the CCADS was not implemented or conceived for craft as small as the IRVE-3, the cables could be appropriated for the new dimensions of a much larger entry vehicle.

3. Shape Morphing Feasibility

Shape morphing is physically possible because the HIAD itself is able to flex to a certain degree without compromising the thermal protection system. This situation offers the unique ability to morph the aerodynamic profile of the HIAD. Altering the profile of an object in a moving fluid will affect its key characteristics, such as lift, drag, and moment. The CCADS is designed to take advantage of this principle and will use shape morphing as its primary control method via cables that deform the profile through controlled tension.

3.1 Evaluation

While experimental validation regarding the effectiveness of shape morphing blunt bodies at high Mach numbers has yet to be accomplished, analysis using Newtonian Impact Theory shows that shape morphing offers an effective amount of control for entry, descent, and landing purposes [1]. In the simulation, the HIAD was modeled using super ellipses and by using this model, the morphing of the HIAD can be described by changing parameters such as eccentricity (e) and corner roundness (n_2). The HIAD system configurations modeled via super ellipses are shown below:

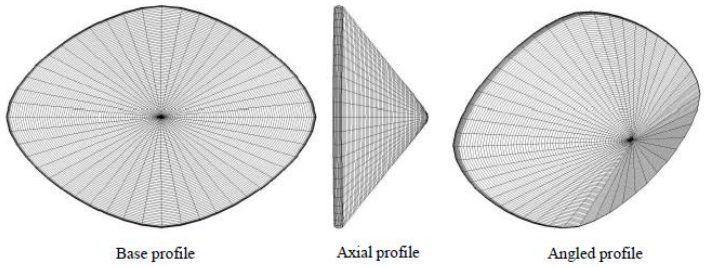

Figure 6. Morphed Aeroshell with e =- 0.7, n_2 = 1.75. [1]

By using a strategic number and placement of cables, the CCADS should be able to morph itself from the spherically blunted profile to a morphed aeroshell, such as in Figure 1. An interesting challenge presents itself in choosing a number of cables that will provide sufficient control over the aeroshell's shape while simultaneously avoiding the negative effects of both the clutter and extra weight of unnecessary cables. The CCADS will utilize between eight and twelve cables equally spaced around the aeroshell in order to deal with these constraints.

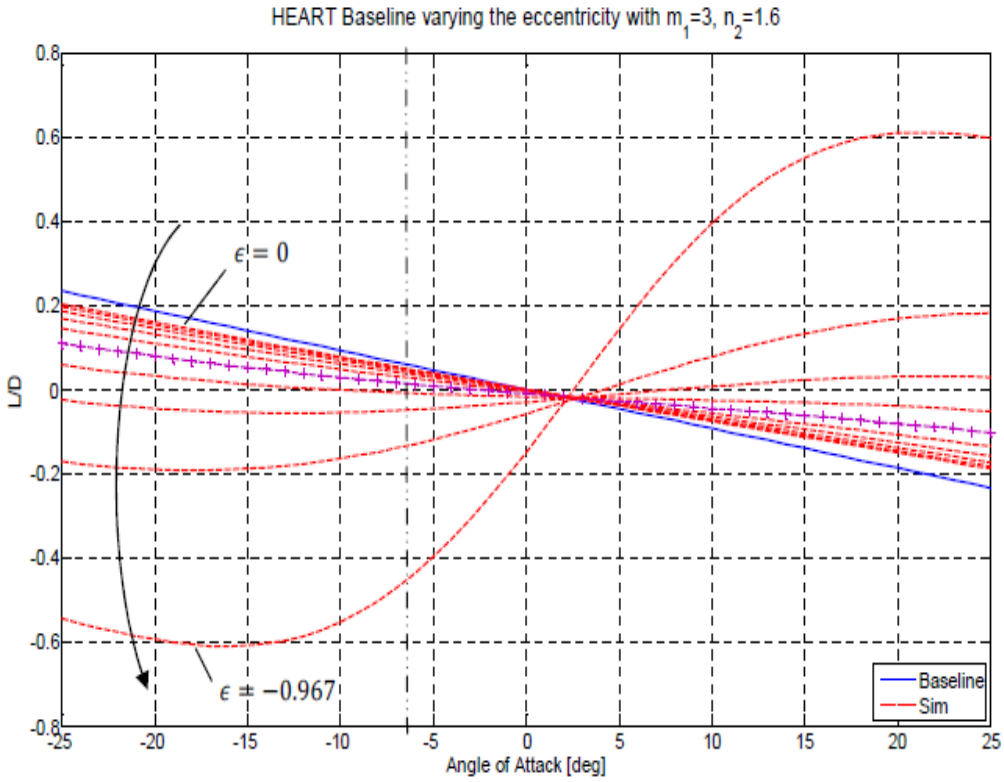

Figure 7. HEART L/D as function of attack and eccentricity. [4]

Simulations show the change in L/D that results from morphing the profile of certain HIADs such as the HEART. By sweeping the eccentricity of HEART, a delta L/D of up to 0.6 can be obtained by using a -10 degree angle of attack. An eccentricity of -0.967 is likely beyond the practical morphing limits of HIADs. This research, however, shows an effective amount of L/D can be controlled by morphing the profile. An interesting caveat of manipulating the L/D in this manner is that the L/D gets increasingly negative as the eccentricity is increased. This can be compensated for by adjusting the trim angle of attack until the desired L/D is achieved.

The advantages of being able to manipulate L/D can be visualized in Figure X4. For a flight path with V_i = 5800m/s, β= 99.5 kg/m^2, γ = -10 deg, it can be observed that changes in L/D result in large changes in range. Through a morphing system, this L/D can be tuned mid-flight to accurately land in a desired landing zone.

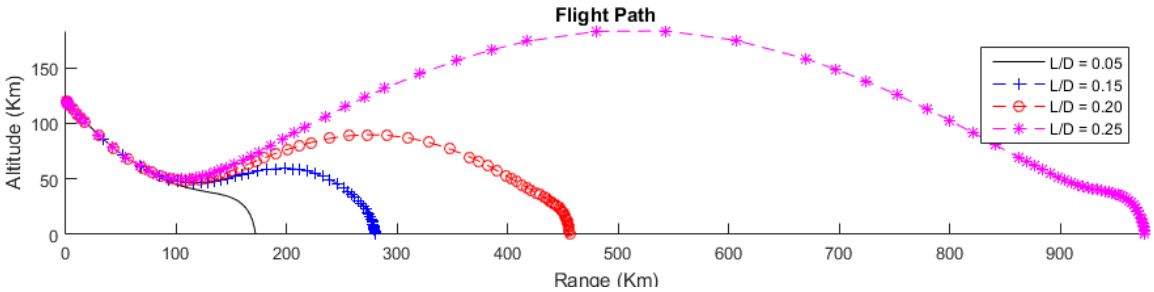

Figure 8. Simulated flight path changes with L/D.

3.2 Simulations, Data, and Graphs

The use of simulations to predict performance has been a big factor in driving design choices. The simulations used have been refined to include planar equations of motion for a planetary entry vehicle. These equations may be written as:

$$\frac{dV}{dt} = -\frac{\rho V^2}{2\beta} - g\sin\gamma \tag{1a}$$

$$\frac{d\gamma}{dt} = -\frac{V\cos\gamma}{R+h} + \frac{\rho V}{2\beta}\left(\frac{L}{D}\right) - \frac{g\cos\gamma}{V} \tag{1b}$$

$$\frac{dh}{dt} = V\sin\gamma \tag{1c}$$

$$\frac{d\Theta}{dt} = \frac{V\cos\gamma}{R+h} \tag{1d}$$

By implementing these planar equations in Matlab, it is possible to observe the expected flight path and velocity profile in order to determine what scenarios to expect and what the final conditions of the flight will be near the end of the descent procedure. The conditions used during this simulation were a ballistic coefficient of 99.5 kg/m^2, an L/D of 0.24, and an entry angle of -11 deg.

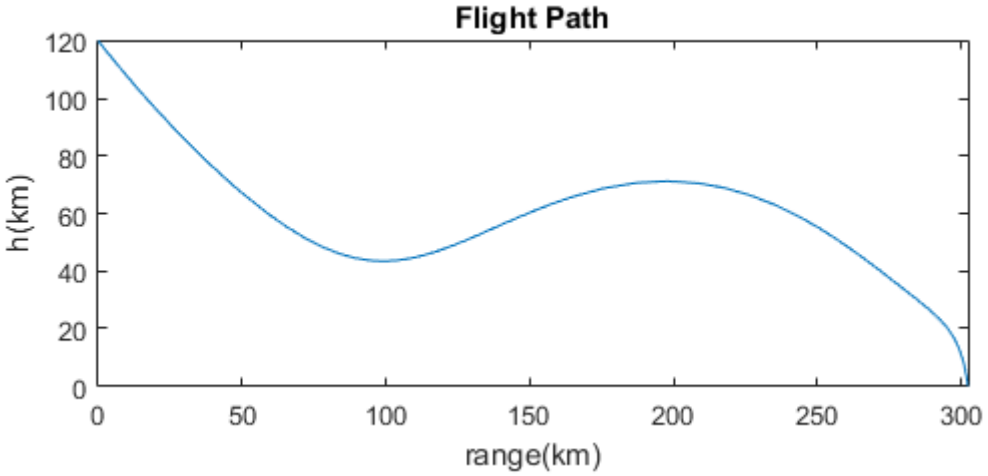

Figure 9. Simulated 2D flight path with V_i = 5800m/s, β= 99.5 kg/m^2, L/D = 0.24, γ = -11 deg.

The simulated flight path reveals that a ballistic coast, or "skip", will occur at an altitude of 45 km at these parameters, thereby increasing the range. By actively controlling the L/D of the entry vehicle through shape morphing, it is possible to reduce or increase the amount of ballistic coast that will occur.

The predicted velocity profile reveals that the entry vehicle will enter a safe terminal descent; this means that the vehicle will be under Mach 1.5 at above 10 km in altitude. This allows ample altitude to deploy parachutes inside their effective region.

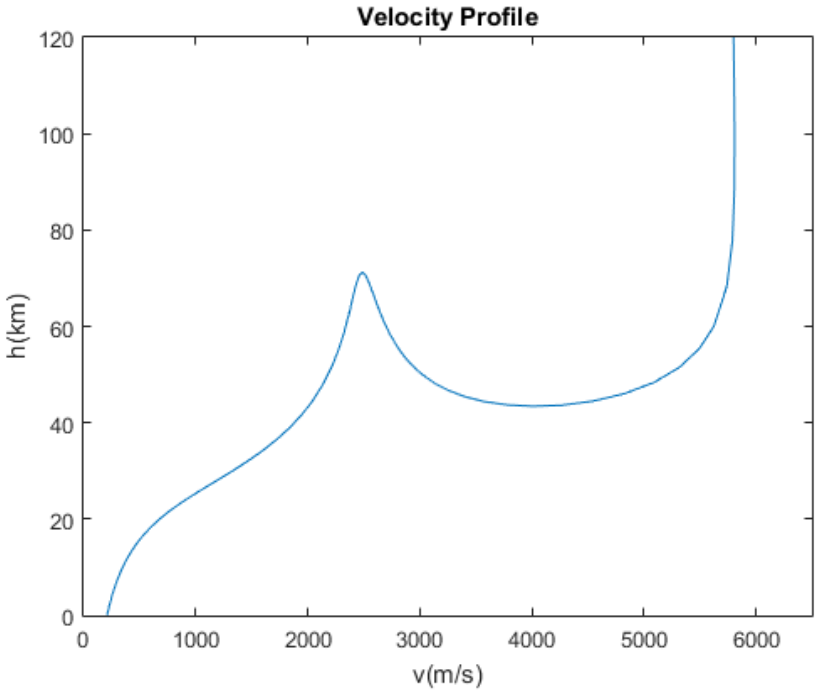

Figure 10. Simulated velocity profile with V_i = 5800m/s, β= 99.5 kg/m^2, L/D = 0.24, γ = -11 deg.

3.3 Analysis of G-Forces and Mitigation Methods

The goal of this research is not only to decelerate massive payloads upon entry into the Mars surface, but also to hopefully facilitate the delivery of human payloads as well. This prompted an analysis of the forces that astronauts would have to endure in this scenario. According to NASA's Human Systems Integration Requirements (HSIR), NASA's limit for G-forces of sustained flight is 4 g's, which is indicated in Figure 7. When the analysis was performed over the time period when deceleration would occur, we concluded that the deceleration would not cause forces higher than 4 g's on the astronauts at any point in the entry window. Therefore, this design and mission profile would be acceptable for human payloads.

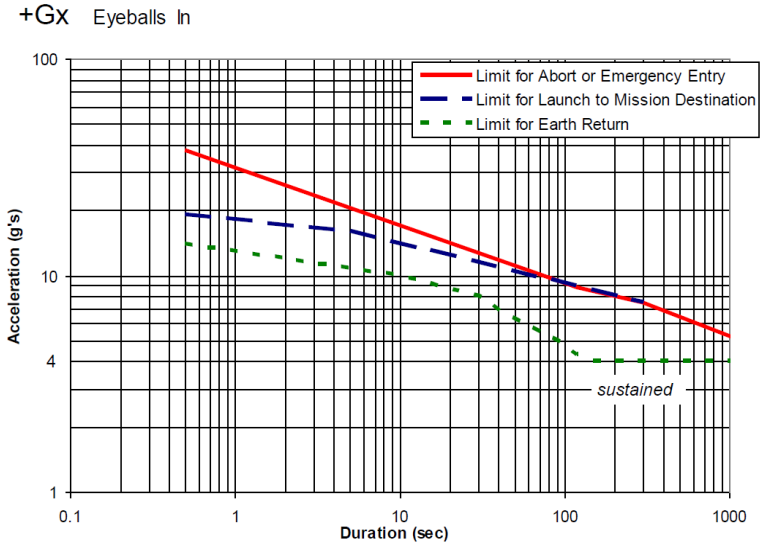

Figure 11. NASA Technical Standard specified max G-force loading on human crew. [6]

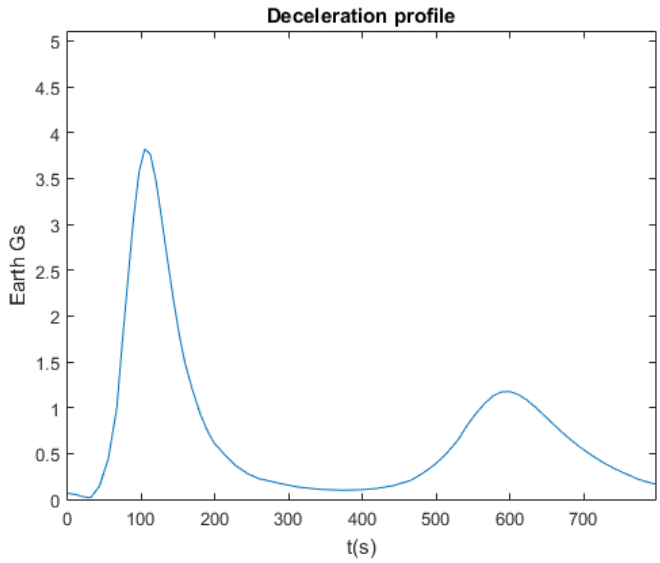

Figure 12. Simulated deceleration profile for V_i = 5800m/s, β= 99.5 kg/m^2, L/D = 0.24, γ = -11 deg.

3.4 Analysis of Expected Heat Flux

Analysis of the expected heat flux has also been conducted. It is assumed that the hottest point on the entry vehicle is at the stagnation point of the tip or "nose" of the aeroshell. Therefore, analysis was focused on this area as it is assumed that if the FTPS is able to survive at this point, then every other point on the FTPS will survive as well. The stagnation point heating can be estimated using the Sutton-Graves method:

$$q = k\sqrt{\frac{\rho}{R_n}}\,V^3 \qquad (2)$$

Where the Sutton-Graves Coefficient for Mars (k) = 1.898 E -4 and the nose or cap radius (R_n) is assumed = 1 meter.

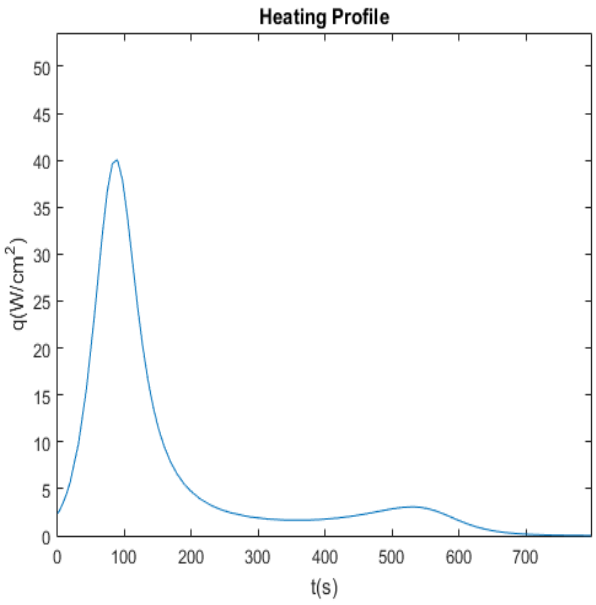

Figure 13. Predicted heat flux for V_i = 5800m/s, β= 99.5 kg/m^2, L/D = 0.24, γ = -11 deg.

The simulation predicts a peak heat flux of approximately 40 Watts/cm^2 and integrating the peak heat flux over the duration of the flight gives a maximum of 4640 Joules/m^2 total heat addition. Second generation FTPS materials such as Nicalon SiC, which can withstand up to 50 W/cm^2, could be used as the outer skin. Nicalon SiC is preferable over the Nextel BF-20 because Nextel is only rated at 30 W/cm^2. The integrated heat loading of 4640 Joules/m^2 is manageable because existing pyrogels, such as pyrogel 6650, with an area of 3.14m^2 and a thickness of 400 microns, will experience a delta-T of 100K. This calculation can be performed using the specific heat equation and the material's properties. Where Q is the integrated heat, c is the material's specific heat, m is material mass, and T is temperature.

$$Q = c \cdot m \cdot \Delta T \tag{3a}$$

$$4640\frac{J}{m^2} \cdot 3.14m^2 = 1.04\frac{J}{g-K} \cdot g \cdot 100K \Rightarrow g = 140g \tag{3b}$$

$$140g \cdot \frac{1}{0.11}\frac{g}{cm^3} \cdot \frac{1}{31400} cm^2 = 0.04cm \; or \; 400 \; microns \tag{3c}$$

4. Technical Readiness Level and Conclusion

The CCADS is a relatively simple, cost-effective HIAD control mechanism that can be purposed for a multitude of Mars missions. Building off the success of previous HIAD technologies, the design prioritizes simplicity in order to attain sufficient control and ease of implementation. Further investigation into cable and shape morphing limits could yield even more versatility to the HIAD, thus making manned interplanetary missions even more feasible.

4.1 Cost Feasibility

A major asset to our CCADS design lies specifically in its mechanical simplicity. All of the technology required to support operation of the CCADS is presently available. None of fundamental aspects of the HIAD design, including the COM and the overall design of the payload compartment have

been modified relative to the initial CCADS concept. he only fundamental aspect of the HIAD design that has been modified is the aeroshell structure configuration; there will be just one giant torus under the FTPS as opposed to multiple stacked tori. The COM and the overall design of the payload compartment, have not been modified relative to the initial CCADS concept.

Trade studies show that Kevlar is an optimal material for the cables. Among other things, Kevlar was chosen for its ability to withstand hysteresis over long periods of time as well as its high specific tensile strength. It is likely that Kevlar cables can withstand the tension required to morph sections of the aeroshell, and the cables would be able to resist the temperatures of entry both at the forebody and at the exposed sections of the HIAD and CCADS, respectively.

The electric motor required for applying tension to the cables is available with current technology, and the only conceivable limit to implementing this technology into the CCADS would be the current size limitations of DC electric motors. In other words, the degree to which the size of conventional, high-powered electric motors would have to be scaled is not yet known, but it is likely that an electric motor concept can be devised to accommodate both the size and power requirements for supporting the CCADS.

4.2 Mission Potential

Implementing the CCADS into HIAD systems would add a new level of flexibility to the guidance and control of Mars entry vehicles. It is capable of changing the flight path of the vehicle at any altitude between 11 and 50 km, enabling precision landing for large payloads. In this way, the CCADS makes the landing process of the entry vehicle safer by providing divert capability. The relative simplicity of the design offers room for many mission-specific alterations that may need to be made to the entry vehicle. The CCADS can achieve softer landings for human missions, or quicker landings for robotic applications where exposure to high G forces is not an issue. A low-mass, reliable system such as the CCADS is exactly what is needed to land large payloads on Mars.

4.3. Technical Readiness Level of the CCADS

Given the amount of information about the CCADS gained through analyses of the system components, operation, and shortcomings in terms of design, the technical readiness level of the the design concept is 2. Despite the fact that no physical models of either the HIAD or CCADS mechanism were created, concentrated effort was made to understand the entry and descent phases of the mission given the dimensions and parameters of the entry vehicle and mission concept. Research into the mission profile and hypersonic behavior of blunted craft both allowed for simulations and analyses of the entry vehicle related to the overall mission concept. These analyses validate the CCADS and show that this mechanism can work in concert with the HIAD to safely transport robotic and human payloads through the atmosphere of Mars.

WORKS CITED

[1] DelCorso, Joseph A., et al. "Flexible Thermal Protection System Development for Hypersonic Inflatable Aerodynamic Decelerators." (2012). International Planetary Probe Workshop 9; 18-22 Jun. 2012; Toulouse; France.

[2] Dillman, Robert, et al. "Flight Performance of the Inflatable Reentry Vehicle Experiment 3." NASA Technical Reports Server (NTRS). NASA, 2013. Web. Feb. 2016.

[3] Downing, James W., Jr., and James A. Newell. "Characterization Of Structural Changes In Thermally Enhanced Kevlar-29 Fiber." Rowan University. Rowan University. Web. 29 Feb. 2016. <http://users.rowan.edu/~newell/Publications/22%20Characterization%20of%20Structural%20Changes.pdf>

[4] Green, James S., Robert E. Lindberg, and Barry J. Dunn. "Morphing Hypersonic Inflatable Aerodynamic Decelerator." Aerospace Research Central. AIAA, 2013. Web. Feb. 2016. <http://arc.aiaa.org/doi/pdf/10.2514/6.2013-1256>.

[5] "Mars Pathfinder: Entry Descent and Landing." Mars Exploration. NASA. Web. 1 Mar. 2016. <http://mars.nasa.gov/MPF/mpf/edl/edl1.html>.

[6] NASA Space Flight Human System Standard—Volume II: Habitability and Environmental Health, NASA-STD-3001, vol. II, 2007.

[7] "Pyrogel® 6650." Insulation Fabricators. Aspen Aerogels. Web. 28 Feb. 2016. <http://www.insulationfabricators.com/downloads/data-sheets/aspen-aerogel-pyrogel-6650-ds.pdf>

[8] "Selection of Electric Motors for Aerospace Applications." NASA Lessons Learned. NASA. Web. 02 Jan. 1999.

[9] "Technical Guide: Kevlar Aramid Fiber." DuPont. DuPont. Web. 22 Feb. 2016. <http://www.dupont.com/content/dam/dupont/products-and-services/fabrics-fibers-and-nonwovens/fibers/documents/Kevlar_Technical_Guide.pdf>.